A Novel Piezoelectric Energy Harvester Using a Multi-Stepped Beam with Rectangular Cavities

Ramalingam Usharani [1], Gandhi Uma [2,*], Mangalanathan Umapathy [2] and Seung-Bok Choi [3,*]

[1] Department of Instrumentation and Control Engineering, Seshasayee Institute of Technology, 620010 Tiruchirappalli, India; ushar.69@gmail.com
[2] Department of Instrumentation and Control Engineering, National Institute of Technology, 620010 Tiruchirappalli, India; umapathy@nitt.edu
[3] Department of Mechanical Engineering, Inha University, 22212 Incheon, Korea
* Correspondence: guma@nitt.edu (G.U.); seungbok@inha.ac.kr (S.-B.C.)

check for updates

Abstract: In vibration-based piezoelectric energy harvesters, one of the major critical issues is increasing the bandwidth and output voltage simultaneously. This manuscript explores a new technique for broadening the operating frequency range and enhancing the output voltage of the piezoelectric material-based energy harvester by appropriate structural tailoring. The wide bandwidth and the improvement in harvested output are accomplished by means of a multi-stepped cantilever beam shaped with rectangular cavities. The harvester is mathematically modeled and analyzed for modal characteristics. It was demonstrated from the outcome that the first two consecutive mode frequencies could be brought closer and the output power was large at both the resonant frequencies compared to the regular cantilever beam energy harvester. The results obtained from experimentation were in agreement with analytical results.

Keywords: piezoelectric energy harvester; multi-stepped cantilever beam; modal characteristics; closer resonance frequency; rectangular cavity

1. Introduction

In the last decade, researchers in all disciplines have evoked great interest in harvesting energy from ambient sources, which were otherwise unutilized. Among various sources such as vibration, solar, wind and thermal considered for energy harvesting, the most attractive source is vibration because of its availability in all environments. Vibration can be used to source wireless sensor systems and researchers across the world are working towards its possible use in industrial condition monitoring systems, medical implants, and smart clothing. Most energy harvesters based on vibration are linear generators that generate power efficiently only at their resonant frequency or near their resonant frequency. In practice, the use of linear generators is limited as they are inefficient at harvesting energy from the frequency-varying ambient vibrations. Hence, in recent years, to overcome this limitation, more focus has been given towards designing vibration-based energy harvesters having wider bandwidth and high output.

The techniques to broaden the operating frequency range are reviewed and presented in References [1,2]. The harvester design presented in Reference [3] widened the bandwidth by appropriately connecting several piezoelectric bimorphs with different resonant frequencies. A special structure having a 'L' shaped beam was presented in Reference [4] featuring the first two natural frequencies that were closer to achieving broadband energy harvesting. In the harvester design reported in Reference [5], the wide bandwidth was achieved by elastically and electrically coupling two identical beams with adjustable and close resonant frequencies. A novel two-degrees-of-freedom

(2DOF) based harvester proposed in Reference [6] provided wider bandwidth compared to the typical Single-degree-of-freedom (SDOF). The harvester design had an outer primary beam and inner cut beam with tip mass. The tip mass was varied to achieve wider bandwidth. The harvester proposed in Reference [7] was designed with a clamped-clamped primary beam bonded with a piezoelectric composite and multiresonant secondary beams attached to one side of the primary beam. The multiresonant response of the secondary beams induced wide band output in the primary beam. The harvester design presented in Reference [8] consisted of a flexible rectangular frame with low Young's modulus in which a series of cantilevers were interdigitally bonded. It provided a multiresonant response and showed a larger bandwidth compared to a conventional cantilever beam. A harvester designed with a dual cantilever with tip mass was reported in Reference [9] in which the resonance frequency was widened by a sliding system having two slanting springs connected to the tip mass. The broadband energy harvester focusing on the dynamic compressive loading was presented in Reference [10]. The flexible slim beam and the applied non-linear axial magnetic force enhanced the output voltage and broadened the bandwidth. A stiffness tunable piezoelectric energy harvester was reported in Reference [11] to achieve high power in the broadband range. Subsequently, the energy harvester with tuning and coupling magnets proposed in Reference [12] could tune the natural frequency to the operating conditions. A new 2D tunable energy harvester based on vibration and featuring transverse and axial stiffness tuning capability was proposed in Reference [13]. The techniques proposed in [14–19] focused on the increment of the output by shaping different cavities in the structure and splitting the beams of smaller size. Piezoelectric broadband energy harvesters having a propped cantilever beam with variable overhang length as host structure was proposed in References [20–23] to get high output over a wide range of operating frequencies. The required bandwidth of the harvester was obtained by varying the support position. Two different structural tailoring approaches namely introduction of step section and cavities are employed to improve the magnitude of the harvested output with the change in operational frequency. Harvester design featuring two tapered beams with and without a cavity was proposed in Reference [24] to obtain high output in wideband simultaneously. The first two-mode frequencies were adjacent with improved output in both the modes. The harvester design proposed in Reference [25] used bimorph PZT films on Ni foil in a piezoelectric compliant mechanism to efficiently extract energy from low frequency vibrations. The strategy for enhancing the performance of the harvester using piezoelectric nano composite was presented in Reference [26]. The piezoelectric nanogenerator reported in Reference [27] showed that by properly choosing the shape of the driving force, the generator output could be enhanced. A harvester which utilizes mass tuning method for bandwidth enhancement was reported in Reference [28]. A harvester with an enhanced frequency bandwidth was presented in Reference [29], which used three bimorphs interconnected by two springs with three end masses. The research problem on energy harvesting for simultaneously achieving broad bandwidth and enhanced output is uncommon. In a harvester that has a normal cantilever beam with uniform dimension, the output is high only in the first mode of vibration. Higher mode frequencies are very far away compared to the first mode and harvesting power in these modes is very difficult.

In this work, to improve the bandwidth and output simultaneously, a new broadband piezoelectric energy harvester designed using a multi-stepped cantilever beam shaped with rectangular cavities is proposed, which is the first research report of its kind. It has adjacent first two-mode frequencies with an enhanced output in both modes. In the regular cantilever beam harvester, the second resonant frequency is about 6.27 times higher than the first mode, whereas in the harvester proposed in this work it is 1.69 times higher than the first mode. This kind of harvester offers higher output both in the first two consecutive modes. This was proven through both an analytical model and an experimental test.

2. Harvester System Overview

The harvester designed using a multi-stepped cantilever beam with rectangular cavities is shown in Figure 1a. Broad bandwidth and enhancement in the output was achieved by introducing multiple

steps and rectangular cavities in the structure. Three piezoelectric patches were attached on the beam and positioned between L_1 and L_2, L_3 and L_4 and L_6 and L_7. The piezoelectric patches were fastened to the maximum strain region of the harvesting structure. The harvester was divided into sections I–VIII as shown in Figure 1a. Sections I, III, V, VI and VIII had only a regular beam. Sections II, IV and VIII were composite sections having a regular beam attached with piezoelectric patches. To increase the strain, rectangular cavities in the thickness direction was shaped in sections II and IV. Three piezoelectric patches were connected appropriately to obtain high output. The harvester performance was assessed by a tip exciter [30].
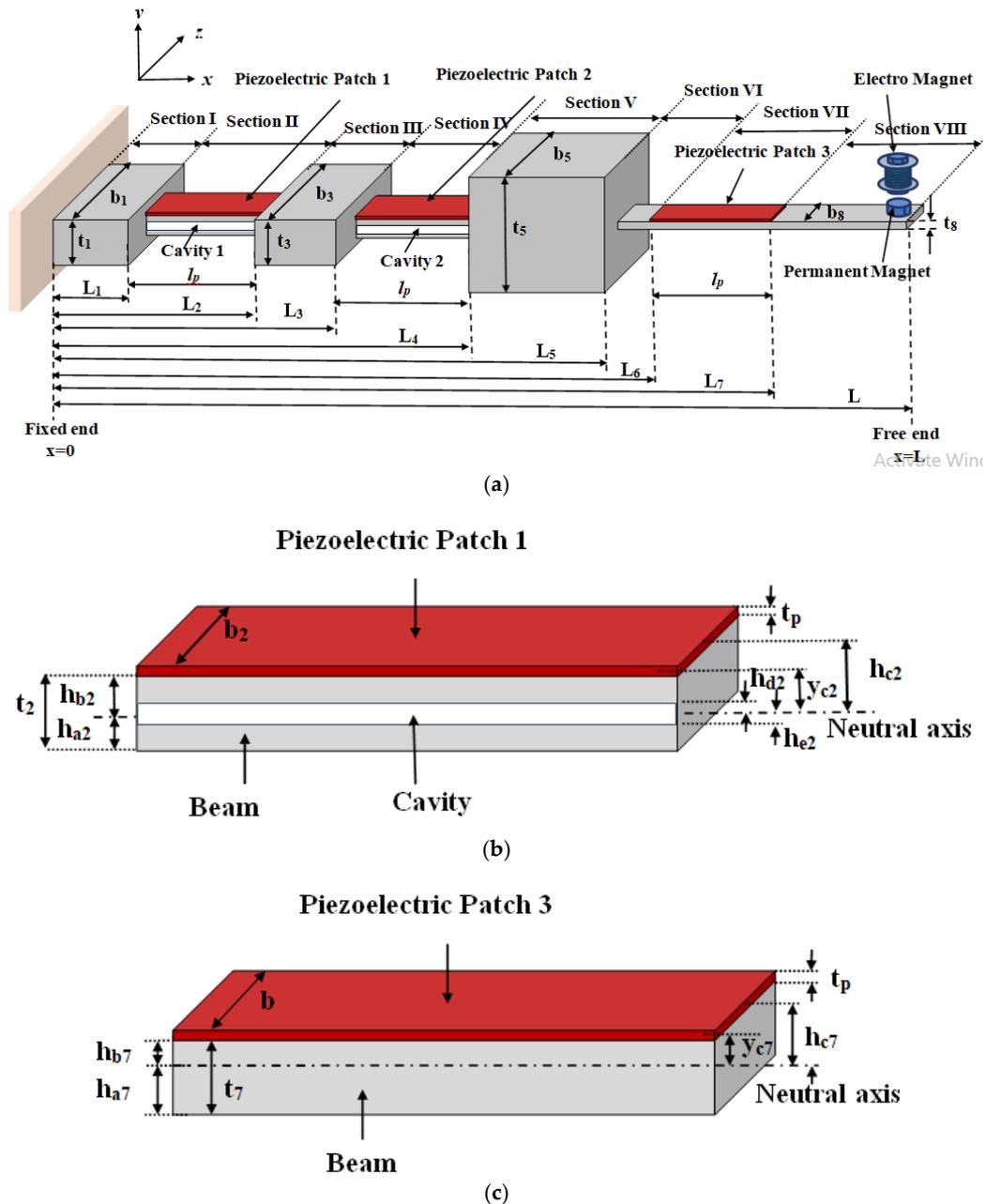
Figure 1. Harvester; (**a**) structure, (**b**) sections II and IV, (**c**) section VII.

3. Analytical Modeling

The modeling of the harvester was carried out using the Euler Bernoulli beam theory. The harvester was made to vibrate at its natural frequency by applying a point tip force $f(x,t) = F\sin(\omega t)\delta(x - L)$

with angular frequency ω and magnitude F. x representing the position on the beam between the fixed and free end ($0 \leq x \leq L$). The Dirac delta function $\delta(x - L)$ was used to model a point force [31]. The electric charge (Q) generated on the surface of the piezoelectric patch 1, 2 and 3 bonded between L_1 and L_2, L_3 and L_4 and L_6 and L_7 and were found as follows [32]:

$$Q_1^{(r)}(t) = -\int_{L_1}^{L_2} \left(d_{31} y_2 E_p b_2 \frac{\partial^2 w_2^{(r)}(x,t)}{\partial x^2} \right) dx \tag{1}$$

$$Q_2^{(r)}(t) = -\int_{L_3}^{L_4} \left(d_{31} y_4 E_p b_4 \frac{\partial^2 w_4^{(r)}(x,t)}{\partial x^2} \right) dx \tag{2}$$

$$Q_3^{(r)}(t) = -\int_{L_6}^{L_7} \left(d_{31} y_7 E_p b_7 \frac{\partial^2 w_7^{(r)}(x,t)}{\partial x^2} \right) dx \tag{3}$$

where d_{31} is the piezoelectric charge coefficient, E_p is the Young's modulus of piezoelectric patches, b_2, b_4 and b_7 are the width of patch 1, 2 and 3, y_2, y_4 and y_7 are the distance between midpoints of the patches to the neutral axis, $w_2^{(r)}(x,t)$, $w_4^{(r)}(x,t)$ and $w_7^{(r)}(x,t)$ are the rth mode transverse displacement of the beam at sections II, IV and VII.

The transverse displacement $w(x,t)$ of the beam was solved using the method of separation of variables [23].

$$w(x,t) = \sum_{r=1}^{\infty} W^{(r)}(x) T^{(r)}(t) \tag{4}$$

where $W^{(r)}(x)$ denotes the spatial mode shape function, $T^{(r)}(t)$ represents the generalized time-dependent coordinate for the rth mode. Substituting Equation (4) into Equations (1)–(3), the charge can be rewritten as follows:

$$Q_1^{(r)}(t) = -d_{31} y_2 E_p b_2 \left[\left. \frac{dW_2^{(r)}(x)}{dx} \right|_{x=L_2} - \left. \frac{dW_2^{(r)}(x)}{dx} \right|_{x=L_1} \right] T_1^{(r)}(t) \tag{5}$$

$$Q_2^{(r)}(t) = -d_{31} y_4 E_p b_4 \left[\left. \frac{dW_4^{(r)}(x)}{dx} \right|_{x=L_4} - \left. \frac{dW_4^{(r)}(x)}{dx} \right|_{x=L_3} \right] T_2^{(r)}(t) \tag{6}$$

$$Q_3^{(r)}(t) = -d_{31} y_7 E_p b_7 \left[\left. \frac{dW_7^{(r)}(x)}{dx} \right|_{x=L_7} - \left. \frac{dW_7^{(r)}(x)}{dx} \right|_{x=L_6} \right] T_3^{(r)}(t) \tag{7}$$

The spatial mode shape function $W^{(r)}(x)$ was solved by using the free undamped vibration governing equation [33]:

$$(EI)_i \frac{d^4 W_i^{(r)}(x)}{dx^4} = \omega_r^2 m_i W_i^{(r)}(x), \ L_{i-1} \leq x \leq L_i \tag{8}$$

where $i = 1, 2, \ldots 8$ $L_0 = 0$, $L_8 = L$

The free vibration solution of Equation (8) was given by:

$$W_i^{(r)}(x) = A_i^{(r)} \sin \beta_i^{(r)} x + B_i^{(r)} \cos \beta_i^{(r)} x + C_i^{(r)} \sinh \beta_i^{(r)} x + D_i^{(r)} \cosh \beta_i^{(r)} x \tag{9}$$

where $\beta_i^{(r)4} = \frac{\omega_r^2 m_i}{(EI)_i}$, $i = 1, 2, \ldots 8$

$A_i^{(r)}, B_i^{(r)}, C_i^{(r)}, D_i^{(r)}$ are unknown constants for the *r*th mode. $\beta_i^{(r)}$'s of each section can be replaced with a single parameter $\beta^{(r)}$.

$$\beta_i^{(r)} = \beta^{(r)} \alpha_i, \ i = 1, 2, \ldots 8 \tag{10}$$

where $\alpha_i = \left(\frac{m_i (EI)_1}{m_1 (EI)_i} \right)^{\frac{1}{4}}$, $\alpha_1 = 1$ and $\beta^{(r)} = \beta_1^{(r)}$.

The flexural rigidity $(EI)_j$ and the mass per unit length (m_j) of sections I, III, V, VI and VIII having only beam patch were:

$$(EI)_j = E_b I_j, \ m_j = \rho_b b_j t_j, \ I_j = \frac{b_j t_j^3}{12}, \ j = 1, 3, 5, 6, 8 \tag{11}$$

E_b, ρ_b represents Young's modulus and density of the beam respectively. I_j, b_j, t_j are the moment of inertia, width and thickness of the beam at the aforementioned sections.

Sections II and IV were composite sections having a beam shaped with rectangular cavities and were bonded with piezoelectric patches. The flexural rigidity $(EI)_k$ and the mass per unit length (m_k) of sections II and IV are given by:

$$(EI)_k = \frac{b_k}{3} \left[E_b \left(h_{bk}^3 - h_{ak}^3 - h_{dk}^3 + h_{ek}^3 \right) + E_p \left(h_{ck}^3 - h_{bk}^3 \right) \right] \tag{12}$$

$$m_k = b_k \left[\rho_b (t_k - t_{ck}) + \rho_p t_p \right], \ k = 2, 4 \tag{13}$$

where E_p, ρ_p and t_p are Young's modulus, density and thickness of the piezoelectric patches. Rectangular cavities of thickness t_{ck} were introduced into the beam of thickness t_k. The beam and the piezoelectric patches had equal width (b_k). h_{ak} and h_{bk} was the distance from the top and bottom of the beam to the neutral axis respectively. h_{ck} was the distance from the top of the patch from the neutral axis. h_{dk} and h_{ek} was the distance from the top and the bottom of the cavity to the neutral axis respectively.

$$h_{ak} = - \left[\frac{\psi t_k (t_k - t_{ck}) + 2 t_p t_k + t_p^2}{2 \left(\psi (t_k - t_{ck}) + t_p \right)} \right], \ h_{bk} = \frac{\psi t_k (t_k - t_{ck}) - t_p^2}{2 \left(\psi (t_k - t_{ck}) + t_p \right)} \tag{14}$$

$$h_{ck} = \frac{2 \psi t_p (t_k - t_{ck}) + \psi t_k (t_k - t_{ck})}{2 \left(\psi (t_k - t_{ck}) + t_p \right)}, \ h_{dk} = \frac{(t_k + t_{ck})}{2} + h_{ak}, \ h_{ek} = -(t_{ck} - h_{dk}) \tag{15}$$

$$y_k = t_k + \frac{t_p}{2} + h_{ak}, \ \psi = \frac{E_b}{E_p}, \ k = 2, 4 \tag{16}$$

Section VII consisted of beam elements bonded with a patch. The flexural rigidity $(EI)_7$ and the mass per unit length (m_7) for section VII was:

$$(EI)_7 = \frac{b_7}{3} \left[E_b \left(h_{b7}^3 - h_{a7}^3 \right) + E_p \left(h_{c7}^3 - h_{b7}^3 \right) \right], \ m_7 = b_7 \left[\rho_b t_7 + \rho_p t_p \right] \tag{17}$$

where

$$\left. \begin{array}{ll} h_{a7} = - \left[\frac{t_p^2 + 2 t_p t_7 + \psi t_7^2}{2 \left(t_p + \psi t_7 \right)} \right], & h_{b7} = \frac{\psi t_7^2 - t_p^2}{2 \left(t_p + \psi t_7 \right)} \\[2mm] h_{c7} = \frac{t_p^2 + 2 \psi t_p t_7 + \psi t_7^2}{2 \left(t_p + \psi t_7 \right)}, & y_7 = \frac{\psi t_7 (t_7 + t_p)}{2 \left(t_p + \psi t_7 \right)} \end{array} \right\} \tag{18}$$

The characteristic matrix equations were formed by substituting the boundary and continuity conditions. The boundary conditions at the fixed and free ends were:

At

$$x = 0, \ W_1^{(r)}(0) = 0, \ \frac{dW_1^{(r)}(0)}{dx} = 0 \tag{19}$$

At

$$x = L, \quad \left. \begin{array}{l} (EI)_8 \dfrac{d^2 W_8^{(r)}(L)}{dx^2} = I_t \omega^2 \dfrac{dW_8^{(r)}(L)}{dx} \\[3mm] (EI)_8 \dfrac{d^3 W_8^{(r)}(L)}{dx^3} = -\omega_r^2 M_t W_8^{(r)}(L) \end{array} \right\} \tag{20}$$

where M_t and I_t represent the mass and inertia of the tip mass respectively.

The continuity conditions at $x = L_q$, where $q = 1, 2, \ldots 7$ was [22]

$$W_q^{(r)}(L_q) = W_{q+1}^{(r)}(L_q), \quad \frac{dW_q^{(r)}(L_q)}{dx} = \frac{dW_{q+1}^{(r)}(L_q)}{dx} \tag{21}$$

$$(EI)_q \frac{d^2 W_q^{(r)}(L_q)}{dx^2} = (EI)_{q+1} \frac{d^2 W_{q+1}^{(r)}(L_q)}{dx^2} \tag{22}$$

$$(EI)_q \frac{d^3 W_q^{(r)}(L_q)}{dx^3} = (EI)_{q+1} \frac{d^3 W_{q+1}^{(r)}(L_q)}{dx^3} \tag{23}$$

Substituting Equations (19)–(23) into Equation (9), the characteristics matrix equation was given by

$$K_{32 \times 32} P_{32 \times 1} = 0 \tag{24}$$

where $K = K(\beta^{(r)})$ was the characteristic matrix and P was the vector of mode shape coefficients. The values of the unknown constants were obtained by solving the characteristic matrix equation of the harvester.

The generalized time-dependent coordinate $T^{(r)}(t)$ for the rth mode was given by [23]

$$T_z^{(r)}(t) = \frac{(W_8^{(r)}(L)F - \chi_z V_z) \sin(\omega t)}{\Delta(\omega_r^2 - \omega^2 + j2\zeta \omega_r \omega)}, \quad z = 1, 2, 3 \tag{25}$$

where χ_z was the modal coupling term [34]:

$$\left. \begin{array}{l} \chi_1 = \vartheta_1 \left[\left. \dfrac{dW_2^{(r)}(x)}{dx} \right|_{x=L_2} - \left. \dfrac{dW_2^{(r)}(x)}{dx} \right|_{x=L_1} \right] \\[4mm] \chi_2 = \vartheta_2 \left[\left. \dfrac{dW_4^{(r)}(x)}{dx} \right|_{x=L_4} - \left. \dfrac{dW_4^{(r)}(x)}{dx} \right|_{x=L_3} \right] \\[4mm] \chi_3 = \vartheta_3 \left[\left. \dfrac{dW_7^{(r)}(x)}{dx} \right|_{x=L_7} - \left. \dfrac{dW_7^{(r)}(x)}{dx} \right|_{x=L_6} \right] \end{array} \right\} \tag{26}$$

$$\vartheta_1 = \frac{E_p d_{31} b_2}{2 t_p} (h_{b2}^2 - h_{c2}^2), \vartheta_2 = \frac{E_p d_{31} b_4}{2 t_p} (h_{b4}^2 - h_{c4}^2), \vartheta_3 = \frac{E_p d_{31} b_7}{2 t_p} (h_{b7}^2 - h_{c7}^2) \tag{27}$$

The voltage $v_z(t)$ and current $i_z(t)$ generated from the patch 1, 2 and 3 were

$$v_z(t) = \frac{Q_z^{(r)}(t)}{C_{pz}}, \quad i_z(t) = \frac{dQ_z^{(r)}(t)}{dt}, \quad z = 1, 2, 3 \tag{28}$$

where $C_{p1} = \frac{\varepsilon_{33}^s b_2 l_p}{t_p}$, $C_{p2} = \frac{\varepsilon_{33}^s b_4 l_p}{t_p}$ and $C_{p3} = \frac{\varepsilon_{33}^s b_7 l_p}{t_p}$ represented the capacitance of the piezoelectric patches. l_p, t_p and ε_{33}^s represented the length, thickness and permittivity of the piezoelectric patches. The three patches were coupled in series and its electrical equivalent circuit is shown in Figure 2.
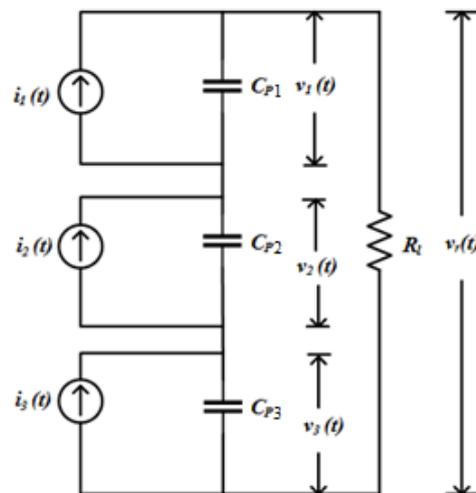
Figure 2. Electrical equivalent circuit of piezoelectric patches.

The voltage $v_1(t)$, $v_2(t)$ and $v_3(t)$ was determined by applying the Kirchhoff current law, as explained below

$$\frac{v_1(t)}{R_l} + C_{p1}\frac{dv_1(t)}{dt} + \frac{v_2(t)}{R_l} + \frac{v_3(t)}{R_l} = i_1(t) \tag{29}$$

$$\frac{v_1(t)}{R_l} + \frac{v_2(t)}{R_l} + C_{p2}\frac{dv_2(t)}{dt} + \frac{v_3(t)}{R_l} = i_2(t) \tag{30}$$

$$\frac{v_1(t)}{R_l} + \frac{v_2(t)}{R_l} + \frac{v_3(t)}{R_l} + C_{p3}\frac{dv_3(t)}{dt} = i_3(t) \tag{31}$$

Let $T_z^{(r)}(t) = T_z^{(r)}e^{j\omega t}$ and $v_z(t) = V_z e^{j\omega t}$, $z = 1, 2, 3$.

The load voltage was computed by solving Equations (29)–(31) and the above equations could be expressed as

$$\left(\frac{1}{R_l} + j\omega C_{pz}\right)V_z - j\omega\sum_{r=1}^{\infty}k_z T_z^{(r)}(t) = 0, z = 1,2,3 \tag{32}$$

Substituting the modal response function from Equation (25) into Equation (32), $v_z(t)$ is obtained as below

$$\left(\frac{1}{R_l} + j\omega C_{pz}\right)V_z - j\omega\sum_{r=1}^{\infty}k_z\frac{(W_8^{(r)}(L)F - \chi_z V_z)}{\Delta(\omega_r^2 - \omega^2 + j2\xi\omega_r\omega)} = 0 \, , \, z = 1,2,3 \tag{33}$$

$$v_z(t) = \frac{\displaystyle\sum_{r=1}^{\infty}\frac{j\omega k_z F W_8^{(r)}(L)}{\Delta(\omega_r^2 - \omega^2 + j2\xi\omega_r\omega)}}{\frac{1}{R_l} + j\omega C_{pz} + \displaystyle\sum_{r=1}^{\infty}\frac{j\omega k_z \chi_z}{\Delta(\omega_r^2 - \omega^2 + j2\xi\omega_r\omega)}}\sin\omega t, \, z = 1,2,3 \tag{34}$$

where

$$F = \frac{N_c I A_c B_p}{2L_{em}}\left(\frac{L_{pm} + d}{\sqrt{R^2 + (L_{pm} + d)^2}} - \frac{d}{\sqrt{R^2 + d^2}}\right) \tag{35}$$

where the properties and dimensions are same as given in [22].

The voltage generated for the first two consecutive modes $(r = 1, 2)$ were considered and from Equation (34) it was obtained as

$$v_z(t) = \frac{j\omega k_z F R_l W_8^{(r)}(L)}{(1 + j\omega R_l C_{pz})(\Delta(\omega_r^2 - \omega^2 + j2\xi\omega_r\omega)) + j\omega k_z\chi_z R_l}\sin\omega t, \, z = 1,2,3 \tag{36}$$

Let $v_z(t) = V_z \sin(\omega t - \phi_z)$. The magnitude (V_z) and phase (ϕ_z) of the output voltage were

$$V_z = \frac{\omega k_z F R_l W_8{}^{(r)}(L)}{\sqrt{\left(\Delta\left(\omega_r^2 - \omega^2 - 2\xi\omega_r\omega^2 C_{pz}R_l\right)\right)^2 + \left(\Delta 2\xi\omega_r\omega + \Delta\omega\omega_r^2 C_{pz}R_l - \Delta\omega^3 C_{pz}R_l + \omega k_z\chi_z R_l\right)^2}} , \; z = 1,2,3 \tag{37}$$

$$\phi_z = \frac{\pi}{2}\mathrm{sgn}(k_z) - \tan^{-1}\left(\frac{2\Delta\xi\omega_r\omega + \Delta\omega\omega_r^2 C_{pz}R_l - \Delta\omega^3 C_{pz}R_l + \omega k_z\chi_z R_l}{\Delta\left(\omega_r^2 - \omega^2 - 2\xi\omega_r\omega^2 C_{pz}R_l\right)}\right), \; z = 1,2,3 \tag{38}$$

The load voltage $(v_r(t))$ was given by

$$v_r(t) = \sum_{z=1}^{3} v_z(t) \tag{39}$$

where $v_r(t) = V_R \sin(\omega t - \phi)$, V_R was the peak value of the load voltage. The magnitude (V_{ocz}) and phase (ϕ_{ocz}) of the open circuit output voltage $(R_l \to \infty)$ from patch 1, 2 and 3 were

$$V_{ocz} = \frac{\omega k_z F W_8{}^{(r)}(L)}{\sqrt{\left(-\Delta 2\xi\omega_r\omega^2 C_{pz}\right)^2 + \left(\Delta\omega\omega_r^2 C_{pz} - \Delta\omega^3 C_{pz} + \omega k_z\chi_z\right)^2}} , \; z = 1,2,3 \tag{40}$$

$$\phi_{ocz} = \frac{\pi}{2}\mathrm{sgn}(k_z) - \tan^{-1}\left(\frac{\Delta\omega\omega_r^2 C_{pz} - \Delta\omega^3 C_{pz} + \omega k_z\chi_z}{-2\Delta\xi\omega_r\omega^2 C_{pz}}\right), \; z = 1,2,3 \tag{41}$$

$$v_{oc}(t) = \sum_{z=1}^{3} v_{ocz}(t) \tag{42}$$

where $v_{oc}(t) = V_{oc} \sin(\omega t - \phi)$, V_{oc} was the peak value of the open circuit output voltage. The average power (P_g) generated from the energy harvester was given by

$$P_g = \frac{V_{rms}^2}{R_l} \tag{43}$$

where $V_{rms} = \frac{V_R}{\sqrt{2}}$ was the root mean square value of the voltage across the resistive load. The amplitude of the current through the resistive load was computed as $I_{rms} = \frac{V_{rms}}{R_l}$. The value of load resistance at the inflection point $\left(\frac{dP_g}{dR_l} = 0\right)$ gave the optimum load resistance.

4. Simulation Results and Discussions

The harvester performance was assessed using the model derived in Section 3 and shown in Figure 1. In the proposed harvester, five steps were formed at $L_1 = 0.022$ L, $L_2 = 0.187$ L, $L_3 = 0.295$ L, $L_4 = 0.46$ L and $L_5 = 0.568$ L. Patch 1, 2 and 3 were glued at L_1, L_3 and L_6 where the strain was maximum. The dimensions and properties of the beam and patches are given in Tables 1–3. The change in the first two-mode frequencies with the variation in thickness (t_5) and (t_6) is shown in Figure 3.

Table 1. The dimensions of the aluminum beam.

Sections	Length (mm)		Width (mm)		Thickness (mm)	
	Symbol	Value	Symbol	Value	Symbol	Value
I	L_1	10	b_1	40	t_1	10
II	$L_2–L_1$	76.5	b_2	25	t_2	6
III	$L_3–L_2$	50	b_3	40	t_3	10
IV	$L_4–L_3$	76.5	b_4	25	t_4	6
V	$L_5–L_4$	50	b_5	40	t_5	50
VI	$L_6–L_5$	10	b_6	12.5	t_6	2
VII	$L_7–L_6$	76.5	b_7	12.5	t_7	2
VIII	$L_8–L_7$	113.5	b_8	12.5	t_8	2

Table 2. The properties of the aluminum beam.

Symbol	Description	Value	Units
E_b	Young's modulus of the beam	71	GP_a
ρ_b	Density of the beam	2700	$Kg\ m^{-3}$

Table 3. The dimensions and properties of patches (PZT 5H).

Symbol	Description	Value	Units
l_p	Length of patch 1 and 2	76.5	mm
b_2, b_4	Width of patch 1 and 2	25	mm
b_7	Width of patch 3	12.5	mm
t_p	Thickness of patch 1, 2 and 3	0.5	mm
E_p	Young's modulus	47.62	GP_a
ρ_p	Density	7500	$Kg\ m^{-3}$
d_{31}	Piezoelectric charge coefficient	-265	pCN^{-1}

From the result, it was found that the first two-mode frequencies were adjacent with the increase in thickness ratio t_5/t_1 and decrease in thickness ratio t_6/t_1. The mode shape of the proposed harvester, proposed harvester without the cavity and conventional cantilever beam-based energy harvester for the first two consecutive modes are shown in Figure 4.
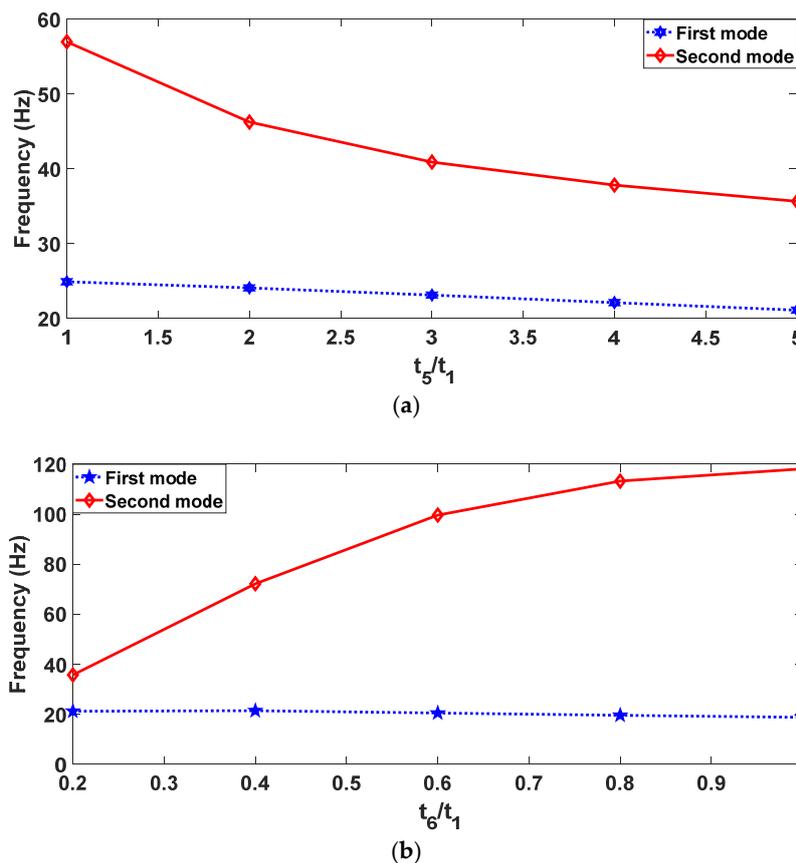
Figure 3. First and second mode frequencies; (**a**) with variation in t_5/t_1, (**b**) with variation in t_6/t_1.
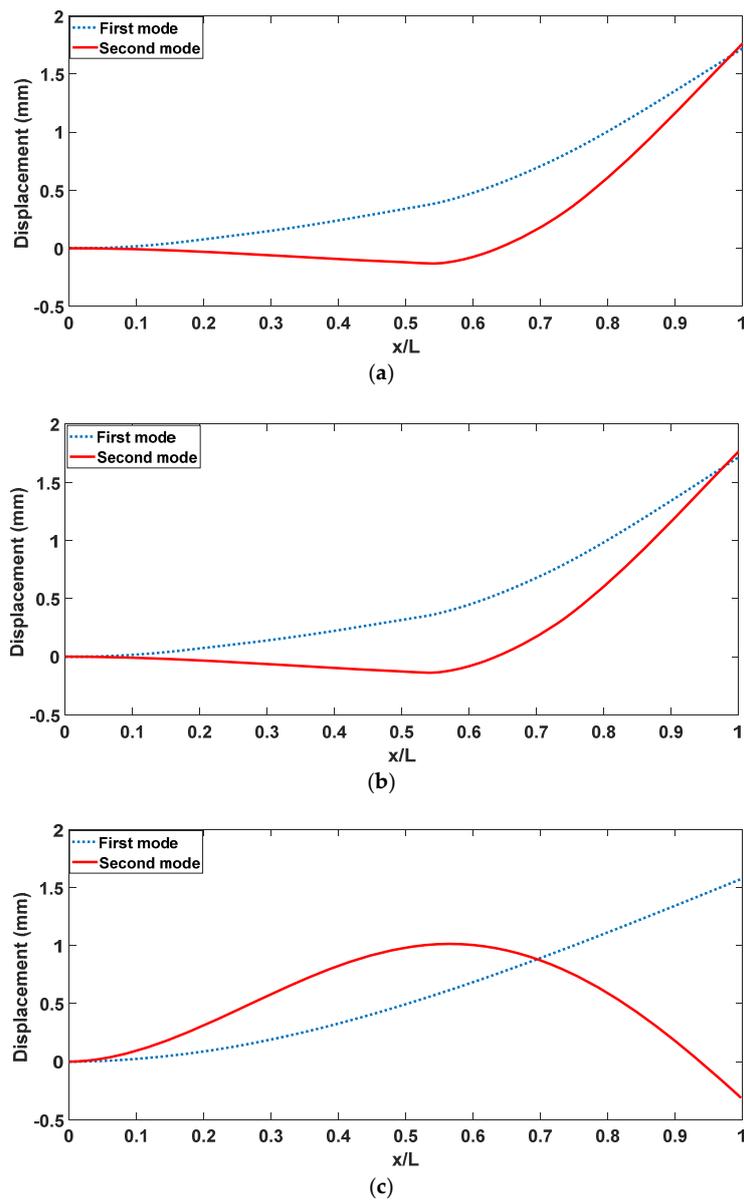
Figure 4. Mode shape; (**a**) proposed harvester, (**b**) proposed harvester without cavity (**c**) conventional cantilever-based harvester.

The output voltage (V_{oc}) from the harvester with no load was computed using Equation (42) given in the modeling section. Figure 5 shows the change in output voltage (V_{oc}), obtained through simulation for the first two modes of vibration. The effectiveness of the proposed harvester's performance was demonstrated by comparing the performance of the harvester having a similar structure without a cavity and also with the regular cantilever-based harvester. The analytical results revealed that in the regular cantilever-based harvester, the output was high only in the first mode of vibration and the second mode frequency was far away from the first mode. The proposed harvester had adjacent first two-mode frequencies with enhanced output in both the modes. From the simulation results, it was observed that in the proposed harvester, the second mode frequency (ω_2) was 1.69 times that of the first mode frequency ($\omega_2 = 1.69\omega_1$) with a high amplitude in both the modes, whereas in the conventional cantilever-based harvester ($\omega_2 = 6.27\omega_1$), the second mode output was very low.
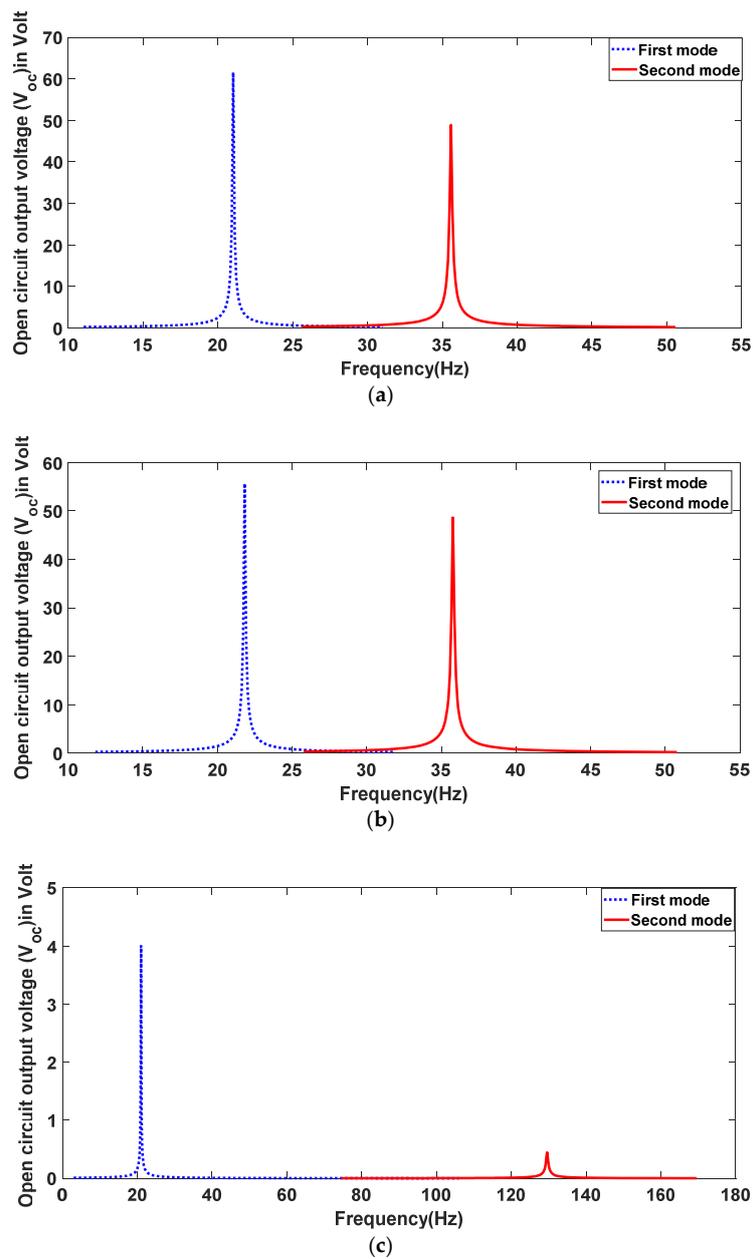
Figure 5. Open circuit output voltage (V_{oc}) (analytical); (**a**) proposed harvester, (**b**) proposed harvester without cavity, and (**c**) conventional cantilever-based harvester.

The load voltage and the average power were computed using Equations (39) and (43) respectively. The power (P_g) was differentiated with respect to the load resistance (R_l) to obtain the optimal load resistance. The value of the load resistance at the inflection point where $\left(\frac{dP_g}{dR_l} = 0 \right)$ was the optimal load resistance. Figure 6 shows the change in load voltage, current and power with the change in load resistance obtained through simulation in the first two consecutive mode resonant frequencies of the proposed harvester. The analytical results presented in Figures 7 and 8 showed the similar performance of the proposed harvester without a cavity and conventional cantilever-based harvester. The analytical results revealed that maximum power was generated at the optimal load resistance in both the modes. In the regular cantilever-based harvester, the power harvested in the second mode was very low whereas in the proposed harvester, the generated power was high and almost equal in both the modes. The proposed harvester not only brings the first two-mode frequencies closer but also

provides enhanced output in both the modes. In the proposed harvester, one of the broadband energy harvesting techniques that is multimodal energy harvesting was implemented.
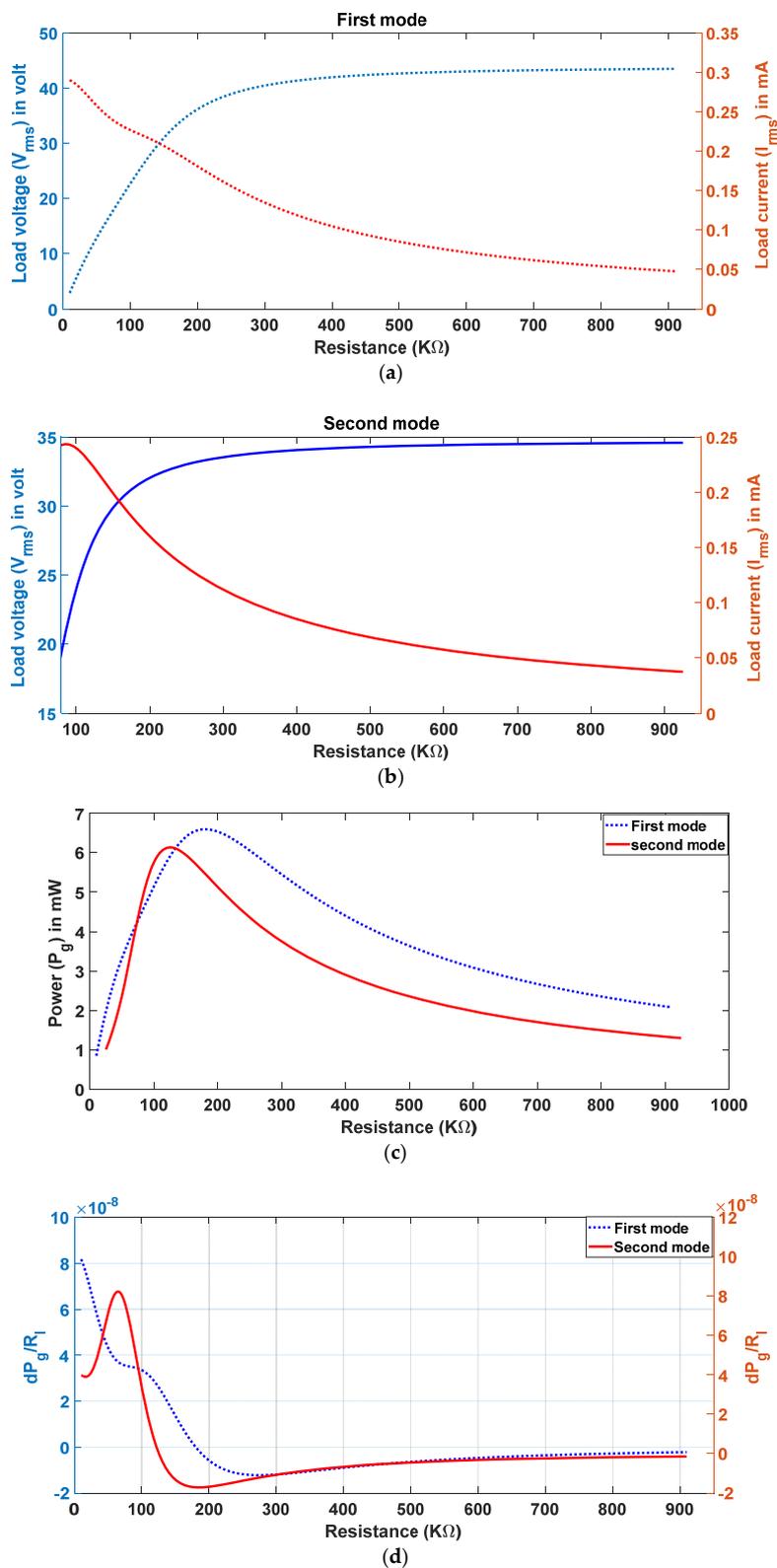
Figure 6. Performance of the proposed harvester with variation in load resistance (analytical); (**a**) variation in voltage and current in the first mode, (**b**) variation in voltage and current in the second mode, (**c**) variation in power and (**d**) variation in the differential of power with respect to R_l.
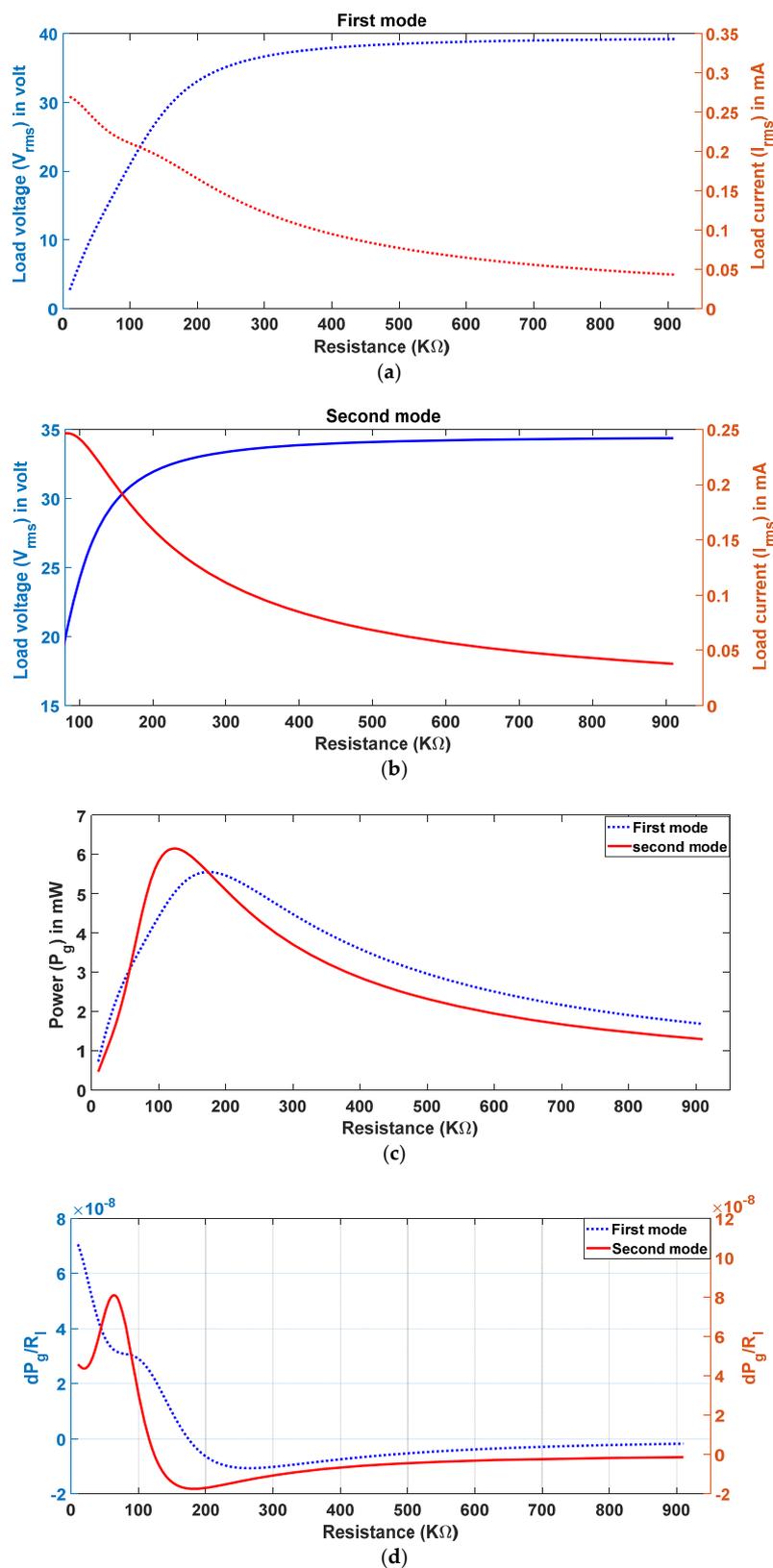
Figure 7. Performance of the proposed harvester without a cavity with variation in load resistance (analytical); (**a**) variation in voltage and current in the first mode, (**b**) variation in voltage and current in the second mode, (**c**) Variation in power and (**d**) variation in the differential of power with respect to R_l.
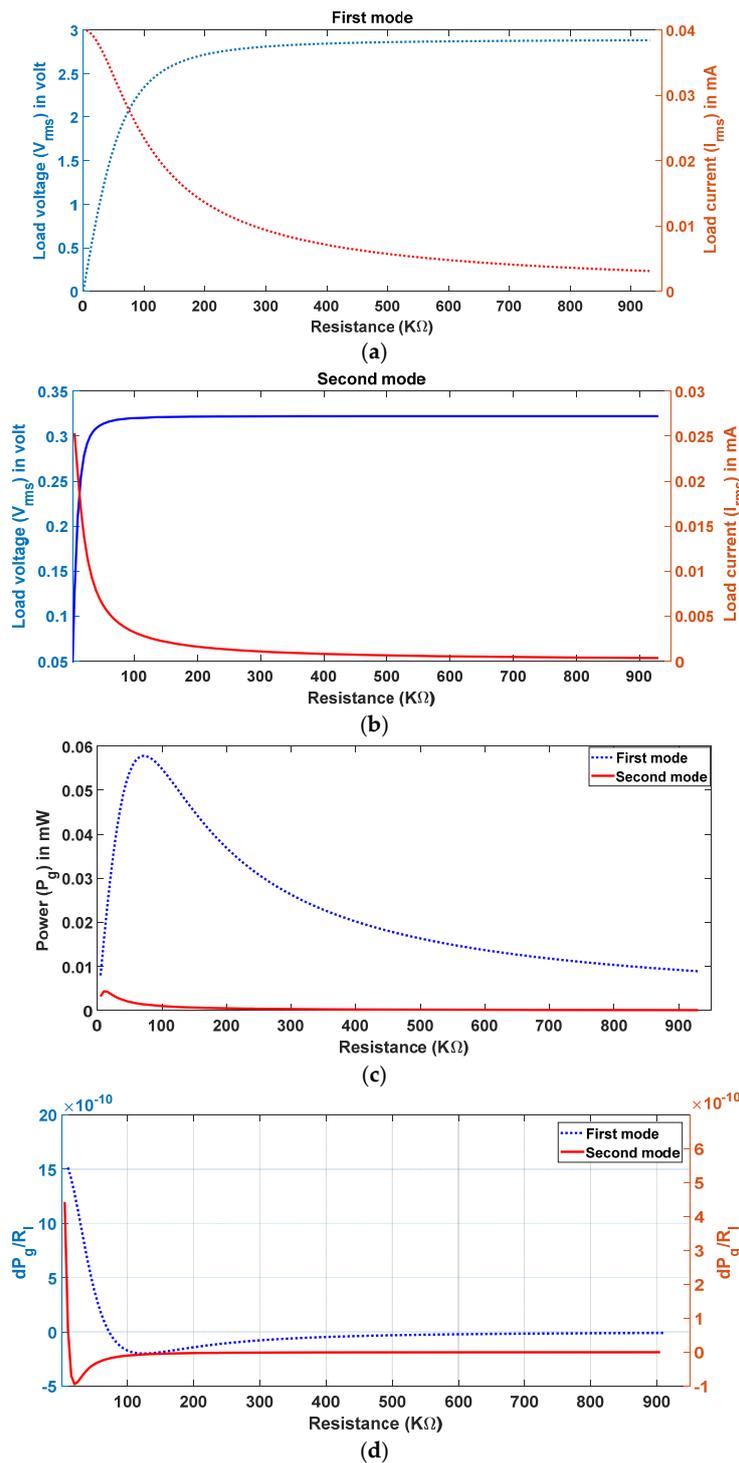
Figure 8. Performance of the conventional cantilever-based harvester with variation in load resistance (analytical); (**a**) variation in voltage and current in the first mode, (**b**) variation in voltage and current in the second mode, (**c**) variation in power and (**d**) variation in the differential of power with respect to R_l.

The analytical results for the proposed harvester are summarized in Table 4 and compared with the results of the harvester having similar structure without a cavity and the conventional cantilever-based energy harvester. From the analytical results presented, it was observed that the proposed harvester provided improved performance in bringing the first two-mode frequencies closer with enhanced output in both the modes.

Table 4. Results from the analytical model.

Proposed Harvester	First Mode					Second Mode				
	F$_1$ (Hz)	V$_{oc}$ (V)	R$_{lopt}$ (KΩ)	V$_R$ (V)	P (mW)	F$_2$ (Hz)	V$_{oc}$ (V)	R$_{lopt}$ (KΩ)	V$_R$ (V)	P (mW)
with step and cavity	21.02	61.55	181	34.46	6.6	35.58	48.85	122	27.69	6.13
with step and without cavity	21.83	55.66	174	31.18	5.56	35.77	48.63	116	27.74	6.15
Conventional Cantilever based harvester	21.02	4.00	72.13	2.16	0.058	129.58	0.45	11.7	0.29	0.0044

5. Experimental Results and Discussion

The harvester with the dimensions given in Tables 1–3 were fabricated and tested. The 2 mm thickness rectangular cavity in the center of the beam was formed by a wire cut EDM tool. To validate the analytical model and results, experimentation was conducted. A photograph of the experimental set up is shown in Figure 9. The function generator was used to apply the required input to the electromagnetic exciter and the output from the patches were observed using DSO (Agilent DSO1002A). The applied excitation signal had a 10 V peak-to-peak amplitude. The dimensions mentioned above were arrived at by simulation of the structure using COMSOL Multiphysics software.

(a)

(b)
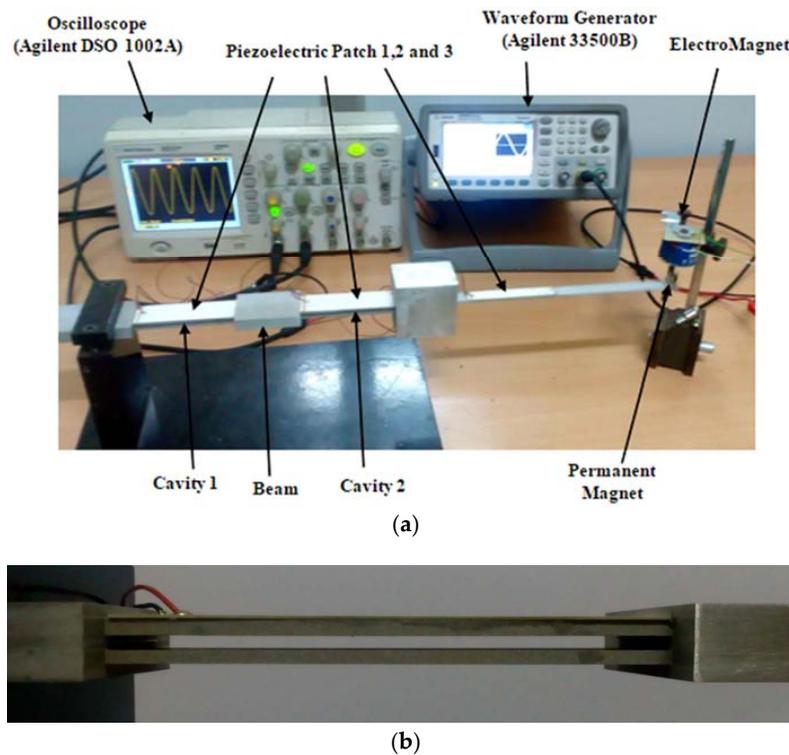
Figure 9. Photograph of the harvester; (**a**) multi stepped beam with cavity and (**b**) view of step with the cavity.

Initially the fabricated harvester was tuned to the first resonant frequency and the open circuit output voltage across the series connected piezoelectric patches were observed. Then, the load resistance was connected and the variation in load voltage with the variation in load resistance was measured. The same steps were repeated by making the harvester vibrate in the second mode frequency. The power was computed using Equation (43) for both the modes. Figure 10 shows a comparison between the harvester output with load in analytical and experimentation.
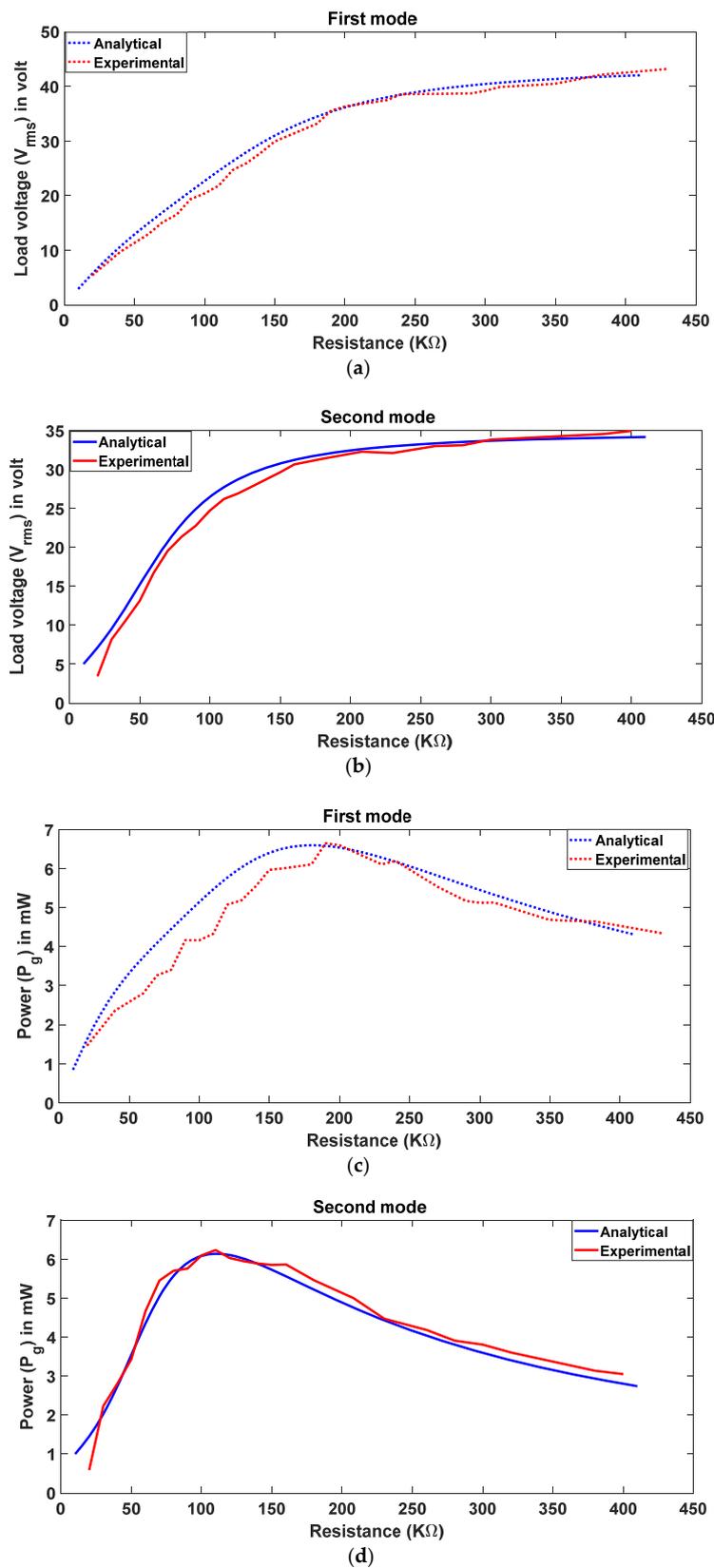
Figure 10. Performance of the proposed energy harvester with variation in load resistance (analytical and experimental); (**a**) variation of voltage in the first mode, (**b**) variation of voltage in the second mode, (**c**) variation of power in the first mode and (**d**) variation of power in the second mode.

Table 5 shows the comparison of the harvester's performance such as resonance frequency, open circuit output voltage, voltage across load resistance and the power obtained through experimentation and analytical modeling. In both the modes, the error computed was less than 5.47%. The results obtained from analytical modeling were in good agreement with experimentation. It was also validated in experimental investigation that the proposed harvester generated higher output wide operating frequency, that is, both in the first and second mode of vibration. Therefore, the energy harvester can be used to power self-sustainable consumer electronics, wireless sensor networks, industrial condition monitoring systems, etc.

Table 5. A comparison of experimental results with analytical results.

Parameter	First Mode			Second Mode		
	Analytical	Experimental	% Error	Analytical	Experimental	% Error
Frequency (Hz)	21.02	20.42	2.85	35.58	34.74	2.35
V_{oc} (V)	61.55	60.1	2.36	48.85	47.6	2.57
V_R (V)	34.46	35.54	3.13	27.69	26.18	5.47
P (mW)	6.6	6.65	0.76	6.13	6.23	1.63

6. Conclusions

Multi-stepped beam based wide operating frequency harvester featuring rectangular cavities was proposed. The results were validated via both computer simulation of the analytical model and experimental investigation. It was shown that in the case of the second mode frequency, the output voltage of the proposed harvester is 1.69 times higher than the first mode of vibration. This results in enhanced power generation of the proposed harvesting structures compared to a conventional cantilever-based energy harvester. By structural tailoring without additional beam or mass, enhanced output in multi modes is achieved. The main benefit of the multi-mode energy harvesting is that, if the dominant frequency of ambient vibration in the environment changes from 20.42 Hz to 34.74 Hz, the proposed harvester will automatically tune to its second mode of vibration (34.74 Hz). In the conventional cantilever with identical first resonant frequency it is not possible, as its second resonant frequency is 6.27 times higher than its first mode and the displacement is very small. The generated voltage from the harvester is more than the conventional harvester, as three piezoelectric patches were attached in the maximum strain region. The harvester has a wide operating frequency range with enhanced output and hence can be used to source consumer electronics, wireless sensor networks and industrial condition monitoring systems etc. The results in terms of resonant frequency and magnitude in both the modes are promising and the next step is to bring the first two frequencies even closer and with more enhanced output. The broadband energy harvester designed with a multi stepped cantilever beam with rectangular cavities can be designed at a micro scale with a conversion and energy storage circuit.

Author Contributions: U.R. designed the idea, performed the analytical modelling and experimental design. U.G. and U.M. validated the analytical and experimental results, drafted the paper. S.-B.C. drafted and revised the paper.

References

1. Zhu, D.; Tudor, M.J.; Beeby, S.P. Strategies for increasing the operating frequency range of vibration energy harvesters: A review. *Meas. Sci. Technol.* **2010**, *21*, 022001. [CrossRef]
2. Tang, L.; Yang, Y.; Soh, C.K. Toward Broadband Vibration-based Energy harvesting. *J. Intell. Mater. Syst. Struct.* **2010**, *21*, 1867–1897. [CrossRef]

3. Xue, H.; Hu, Y.; Wang, Q.M. Broadband piezoelectric energy harvesting devices using multiple bimorphs with different operating frequencies. *IEEE Trans. Ultrason. Ferroelect. Freq. Control* **2008**, *55*, 2104–2108.

4. Erturk, A.; Renno, J.M.; Inman, D.J. Modeling of Piezoelectric Energy harvesting from an L shaped beam mass structure with an application to UAVs. *J. Intell. Mater. Syst. Struct.* **2009**, *20*, 529–544. [CrossRef]

5. Yang, Z.; Yang, J. Connected vibrating Piezoelectric Bimorph beams as a wide-band piezoelectric power harvester. *J. Intell. Mater. Syst. Struct.* **2009**, *20*, 569–574. [CrossRef]

6. Wu, H.; Tang, L.; Yang, Y.; Soh, C.K. A novel two-degrees-of-freedom piezoelectric energy harvester. *J. Intell. Mater. Syst. Struct.* **2013**, *24*, 357–368. [CrossRef]

7. Qi, S.; Shuttleworth, R.; Oyadiji, S.O.; Wright, J. Design of multiresonant beam for broadband piezoelectric energy harvesting. *Smart Mater. Struct.* **2010**, *19*, 094009. [CrossRef]

8. Li, P.; Liu, Y.; Wang, Y.; Luo, C.; Li, G.; Hu, J.; Liu, W.; Zhang, W. Low-frequency and wideband vibration energy harvester with flexible frame and interdigital structure. *AIP Adv.* **2015**, *5*, 047151. [CrossRef]

9. Niri, D.E.; Salamone, S. A passively tunable mechanism for a dual bimorph energy harvester with variable tip stiffness and axial load. *Smart Mater. Struct.* **2012**, *21*, 125025. [CrossRef]

10. Zhu, Y.; Zu, J.; Su, W. Broadband energy harvesting through piezoelectric beam subjected to dynamic compressive loading. *Smart Mater. Struct.* **2013**, *22*, 045007. [CrossRef]

11. Peters, C.; Maurath, D.; Schock, W.; Mezger, F.; Manoli, Y. A closed-loop wide-range tunable mechanical resonator for energy harvesting systems. *J. Micromech. Microeng.* **2009**, *19*, 094004. [CrossRef]

12. Hoffmann, D.; Willmann, A.; Hehn, T.; Folkmer, B.; Manoli, Y. A self-adaptive energy harvesting system. *Smart Mater. Struct.* **2016**, *25*, 035013. [CrossRef]

13. Dong, L.; Prasad, M.G.; Fisher, F.T. Two-dimensional resonance frequency tuning approach for vibration-based energy harvesting. *Smart Mater. Struct.* **2016**, *25*, 065019. [CrossRef]

14. Sang, M.C.; Dayou, J.; Liew, W.Y. Increasing the Output from Piezoelectric Energy Harvester Using Width-Split Method with Verification. *Int. J. Precis. Eng. Man.* **2013**, *14*, 2149–2155. [CrossRef]

15. Dayou, J.; Kim, J.; Im, J.; Zhai, L.; How, A.T.; Liew, W.Y. The effects of width reduction on the damping of a cantilever beam and its application in increasing the harvesting power of piezoelectric energy harvester. *Smart Mater. Struct.* **2015**, *24*, 045006. [CrossRef]

16. Reddy, R.A.; Umapathy, M.; Ezhilarasi, D.; Uma, G. Improved energy harvesting from vibration by introducing cavity in a cantilever beam. *J. Vib. Control* **2014**, *22*, 3057–3066. [CrossRef]

17. Reddy, R.A.; Umapathy, M.; Ezhilarasi, D.; Uma, G. Cantilever Beam with Trapezoidal Cavity for Improved Energy Harvesting. *Int. J. Precis. Eng. Manuf.* **2015**, *16*, 1875–1881. [CrossRef]

18. Reddy, R.A.; Umapathy, M.; Ezhilarasi, D.; Uma, G. Modelling and Experimental investigations on stepped beam with cavity for energy harvesting. *Smart Struct. Syst.* **2015**, *16*, 623–640. [CrossRef]

19. Raju, S.S.; Umapathy, M.; Uma, G. Cantilever piezoelectric energy harvester with multiple cavities. *Smart Mater. Struct.* **2015**, *24*, 115023. [CrossRef]

20. Usharani, R.; Uma, G.; Umapathy, M. Design of High Output Broadband Piezoelectric Energy Harvester with Double Tapered Cavity Beam. *Int. J. Precis. Eng. Manuf. Green Technol.* **2016**, *3*, 343–351. [CrossRef]

21. Usharani, R.; Uma, G.; Umapathy, M.; Choi, S.B. A new broadband energy harvester using propped cantilever beam with variable overhang. *Smart Struct. Syst.* **2017**, *19*, 567–576. [CrossRef]

22. Usharani, R.; Uma, G.; Umapathy, M.; Choi, S.B. A new piezoelectric-patched cantilever beam with a step section for high performance of energy harvesting. *Sens. Actuators A* **2017**, *265*, 47–61.

23. Usharani, R.; Uma, G.; Umapathy, M.; Choi, S.B. Design of high output broadband piezoelectric energy harvester. *J. Mech. Sci. Technol.* **2017**, *31*, 3131–3142. [CrossRef]

24. Usharani, R.; Uma, G.; Umapathy, M.; Choi, S.B. A new piezoelectric energy harvester using two beams with tapered cavity for high power and wide broadband. *Int. J. Mech. Sci.* **2018**, *142–143*, 224–234.

25. Yeo, G.H.; Ma, X.; Rahn, C.; Trolier-McKinstry, S. Efficient Piezoelectric Energy Harvesters Utilizing (001) Textured Bimorph PZT Films on Flexible Metal Foils. *Adv. Funct. Mater.* **2016**, *26*, 5940–5946. [CrossRef]

26. Jeong, K.C.; Baek, C.; Kingon, A.I.; Park, K.; Kim, S.H. Lead-Free Perovskite Nanowire-Employed Piezopolymer for Highly Efficient Flexible Nanocomposite Energy Harvester. *Small* **2018**, *14*, 1704022. [CrossRef] [PubMed]

27. Xu, Q.; Qin, Y. Theoretical study of enhancing the piezoelectric nanogenerator's output power by optimizing the external force's shape. *APL Mater.* **2017**, *5*, 074101. [CrossRef]

28. Dechant, E.; Fedulov, F.; Fetisov, L.Y.; Shamonin, M. Bandwidth widening of piezoelectric cantilever beam arrays by mass-tip tuning for low-frequency vibration energy harvesting. *Appl. Sci.* **2017**, *7*, 1324. [CrossRef]

29. Abramovich, H.; Har-nes, I. Analysis and Experimental Validation of a Piezoelectric Harvester with Enhanced Frequency Bandwidth. *Materials* **2018**, *11*, 1243. [CrossRef] [PubMed]

30. Kumar, B.S.; Suresh, K.; Kumar, U.V.; Uma, G.; Umapathy, M. Resonance based DC current sensor. *Measurement* **2012**, *45*, 369–374. [CrossRef]

31. Wang, Q.; Wu, N. Optimal design of a piezoelectric coupled beam for power harvesting. *Smart Mater. Struct.* **2012**, *21*, 085013. [CrossRef]

32. Chen, N.S.; Wang, G.J.; Chien, M.C. Analytical modeling of piezoelectric vibration-induced micro power generator. *Mechatronics* **2006**, *16*, 379–387. [CrossRef]

33. Salehi-Khojin, A.; Bashash, S.; Jalili, N. Modeling and experimental vibration analysis of nanomechanical cantilever active probes. *J. Micromech. Microeng.* **2008**, *18*, 085008. [CrossRef]

34. Erturk, A. Electromechanical Modelling of Piezoelectric Energy Harvesters. Ph.D. Thesis, Virginia Tech, Blacksburg, VA, USA, 2009.